

Delving into the anisotropic interlayer exchange in bilayer CrI_3

Srdjan Stavrić,^{1,2} Paolo Barone,³ and Silvia Picozzi¹

¹*Consiglio Nazionale delle Ricerche CNR-SPIN, c/o*

Università degli Studi "G. D'Annunzio", 66100 Chieti, Italy

²*Vinča Institute of Nuclear Sciences - National Institute of the Republic of Serbia, University of Belgrade, P. O. Box 522, RS-11001 Belgrade, Serbia**

³*Consiglio Nazionale delle Ricerche CNR-SPIN, Area della Ricerca di Tor Vergata, Via del Fosso del Cavaliere, 100, I-00133 Rome, Italy*

(Dated: May 26, 2023)

Abstract

Bilayer CrI_3 attracted much attention owing to peculiar switching between the layered ferromagnetic and antiferromagnetic order upon stacking alternation. This finding pointed out the importance of the apparently small interlayer exchange, yet, existing literature addresses only its isotropic part. To fill this gap, we combine the density functional theory with Hamiltonian modeling to examine the anisotropic interlayer exchange in bilayer CrI_3 – Dzyaloshinskii-Moriya (DMI) and the Kitaev interaction (KI). We develop and apply a novel computational procedure that yields the off-diagonal exchange matrix elements with μeV accuracy. Inspecting two types of bilayer stacking, we found a weak interlayer KI and much stronger DMI between the sublattices of monoclinic bilayer and their complete absence in rhombohedral bilayer. We show how these anisotropic interactions depend on the interlayer distance, stacking sequence, and the spin-orbit coupling strength and suggest the dominant superexchange processes at play. In addition, we demonstrate that the single-ion anisotropy largely depends on stacking, increasing by 50% from monoclinic to rhombohedral structure. Remarkably, our findings prove that iodines, owing to their spatially extended $5p$ orbitals featuring strong spin-orbit coupling, are extremely efficient in mediating DMI across the van der Waals gap in two-dimensional magnetic heterostructures. Given that similar findings were previously demonstrated only in metallic multilayers where the DMI shows a much longer range, our study gives promise that the chiral control of spin textures can be achieved in two-dimensional semiconducting magnetic bilayers whose ligands feature strong spin-orbit coupling.

I. INTRODUCTION

Since the long sought discovery of two-dimensional (2D) magnets finally happened with CrI_3 and $\text{Cr}_2\text{Ge}_2\text{Te}_6$ ^{1,2}, a large stream of scientific efforts has been directed towards achieving new capabilities with magnetic van der Waals (VdW) heterostructures³⁻⁷. Given the diversity of 2D materials, there is a profusion of possible magnetic VdW heterostructures that offer endless possibilities. Yet, to find intriguing phenomena, one doesn't need to look any further from the two layers of CrI_3 . So far, the magnetic properties of bilayer CrI_3 are manipulated by electric fields^{8,9}, electrostatic doping¹⁰, pressure¹¹, and twisting¹². In addition, theoretical studies proposed to switch the direction of magnetization in one of its layers by spin-orbit torque¹³ and predicted the magnetic photogalvanic effect¹⁴, magnetic polarons¹⁵, and magnetoelectric response in bilayer CrI_3 ¹⁶. Yet, to efficiently exploit the possibilities offered by bilayer CrI_3 in new concept devices, one has to truly understand the mechanism of the exchange coupling between the layers.

Monolayer CrI_3 is composed of chromium atoms arranged in a honeycomb lattice surrounded by edge-sharing iodine octahedra. Below the Curie temperature the $S = 3/2$ spins on Cr atoms are parallel and the monolayer CrI_3 is a ferromagnet (FM) with an out-of-plane magnetization¹⁷⁻¹⁹. The magnetic anisotropy energy (MAE), that is absolutely necessary for the long-range magnetic order to persist in 2D crystals at finite temperatures²⁰, emerges in CrI_3 from an interplay between the single-ion anisotropy (SIA) and the two-ion anisotropy (TIA) occurring between the nearest neighbors Cr ions^{17,21}. The TIA is usually derived within the generalized Heisenberg-Kitaev model and gives rise, in addition to the conventional isotropic Heisenberg exchange, to the Kitaev exchange and to the symmetric pseudo-dipolar interaction, depending on the bond-orientation. These terms, which we will generally label as "Kitaev-like interaction" (KI), refer to the traceless symmetric part of the most general expression for bilinear spin-spin interactions²² and cooperate with dipole-dipole interaction in shaping the total magnetic anisotropy²³. Like SIA, the KI in CrI_3 comes mostly from the spin-orbit coupling (SOC) on iodine atoms. MAE scales with the ligand SOC strength, being instrumental to CrI_3 showing a higher Curie temperature (T_C) than the isostructural CrBr_3 and CrCl_3 , whose ligands feature much weaker SOC than iodines²⁴⁻²⁷. Besides SIA and KI, SOC can give rise to the Dzyaloshinskii-Moriya interaction (DMI). However, the presence of an inversion center in the nearest neighbor Cr-Cr bonds

imposes that this antisymmetric part of the anisotropic exchange is exactly zero. On the other hand the DMI is allowed between the next-nearest Cr neighbors and, although being tiny, it can play an important role in gapping the magnon spectra²⁸.

In addition to magnetic properties that bilayer CrI₃ inherits from its constitutive layers, the interlayer exchange has proven extremely important as it can affect the direction of layers' magnetizations. It is an order of magnitude weaker than the intralayer exchange, but the possibility to tune it via stacking alternations made it a subject of numerous studies. For example, if we adopt the stacking from bulk CrI₃ that crystallizes either in rhombohedral (the low temperature or LT phase, $R\bar{3}$ space group) or monoclinic lattice (the high temperature or HT phase, $C/2m$ space group)²⁹, we end up with two different bilayer structures that we refer to as the LT and the HT structure (Fig. 1a-b). Here the theoretical^{10,30-33} and experimental³⁴ studies agree: the LT stacking favors the FM ordering of layers' magnetizations, whereas the HT stacking leads to layered antiferromagnetic (AFM) order. However, being realized through (at least) two iodines, the interlayer Cr-Cr coupling is mostly of super-superexchange type, which makes its microscopic description complicated due to a high number of relevant hopping processes^{35,36}.

In bilayer CrI₃ studies galore the interlayer exchange is most often considered isotropic. This is a reasonable assumption, given that the bilayer CrI₃ lattice is centrosymmetric and thus the DMI is forbidden, whereas the KI, if nonzero, is usually very small. However, the strict constraints imposed on DMI by the global symmetry of the structure by no means forbid the DMI to appear locally, between the specific neighbors. Moreover, if the DMI exists between the specific neighbors and the global symmetry constraints are somehow removed – the macroscopic DMI can emerge as well. New studies warm up such expectations showing that skyrmions – topologically protected particle-like spin textures that usually appear as a consequence of DMI – can be induced via moire magnetic exchange interactions in twisted bilayer CrI₃^{12,37,38}. Speaking of interlayer DMI in general, Vedmedenko *et al.*³⁹ proposed the atomistic model that predicts the formation of global chiral spin textures due to interlayer DMI between the ferromagnetic layers coupled through a nonmagnetic spacer. Recently, chiral control of spin textures is experimentally achieved in ferromagnetic TbFe/Pt/Co thin films, where the out-of-plane magnetization of TbFe is DMI-coupled with the in-plane magnetization of Co⁴⁰. In this multilayer system the interlayer DMI is strong because the Pt atoms carry the conductive electrons that feature strong SOC. Having this

in mind, the question is whether the iodine ligands, that also have considerable SOC, can play the role of DMI-mediator in bilayer CrI_3 . Moreover, having in mind the importance of KI in monolayer CrI_3 , how strong is the interlayer KI in bilayer CrI_3 ?

We present a theoretical study that combines the density functional theory (DFT) and Hamiltonian modeling in calculating the anisotropic part of the interlayer exchange in bilayer CrI_3 . The manuscript is organized as follows: we start by presenting the employed computational approach in Subsection II A and describe the model Hamiltonian that expresses the coupling between two perpendicular spins in Subsection II B. The ability of the perpendicular-spins model to capture the changes in DFT band energies is demonstrated in Subsection II C. The validity of the model is extended to describe the coupling between fully magnetized layers in Subsection II D, where we reveal a considerable DMI and an order of magnitude weaker KI between the sublattices of bilayer CrI_3 . We demonstrate how both DMI and KI depend on structural transformations and the SOC strength in Subsection II E, suggesting possible superexchange mechanisms governing these interactions. Finally, in Section III we summarize the study by proposing a 2D magnetic heterostructure that should be a suitable platform for realizing the interlayer DMI coupling of layers' magnetizations, similar to that experimentally achieved in metallic thin films.

II. RESULTS

A. Computational approach

We model the bilayer CrI_3 by stacking two CrI_3 layers in rhombohedral (LT) and monoclinic (HT) sequences (Fig. 1). The structural details and computational parameters of DFT calculations are given in the Section IV. In order to study the coupling between the two spins from different layers, we need to isolate them from the rest of the magnetic environment. To solve this problem, we use the 2×2 supercell and replace by Al all the Cr atoms except the two inspected ones (Fig. 1c). Al, like Cr, is trivalent so it doesn't perturb much the surrounding iodine ligand field. Therefore, the two remaining Cr atoms end up embedded into nonmagnetic crystalline environment that is reminiscent of that in bilayer CrI_3 . To check the validity of the atomic replacement method, we calculated the SIA and the intralayer nearest-neighbor exchange tensor \mathcal{J}_1 of monolayer CrI_3 and compared the results to those

obtained with the reference four-state method⁴¹ in Supplementary Information.

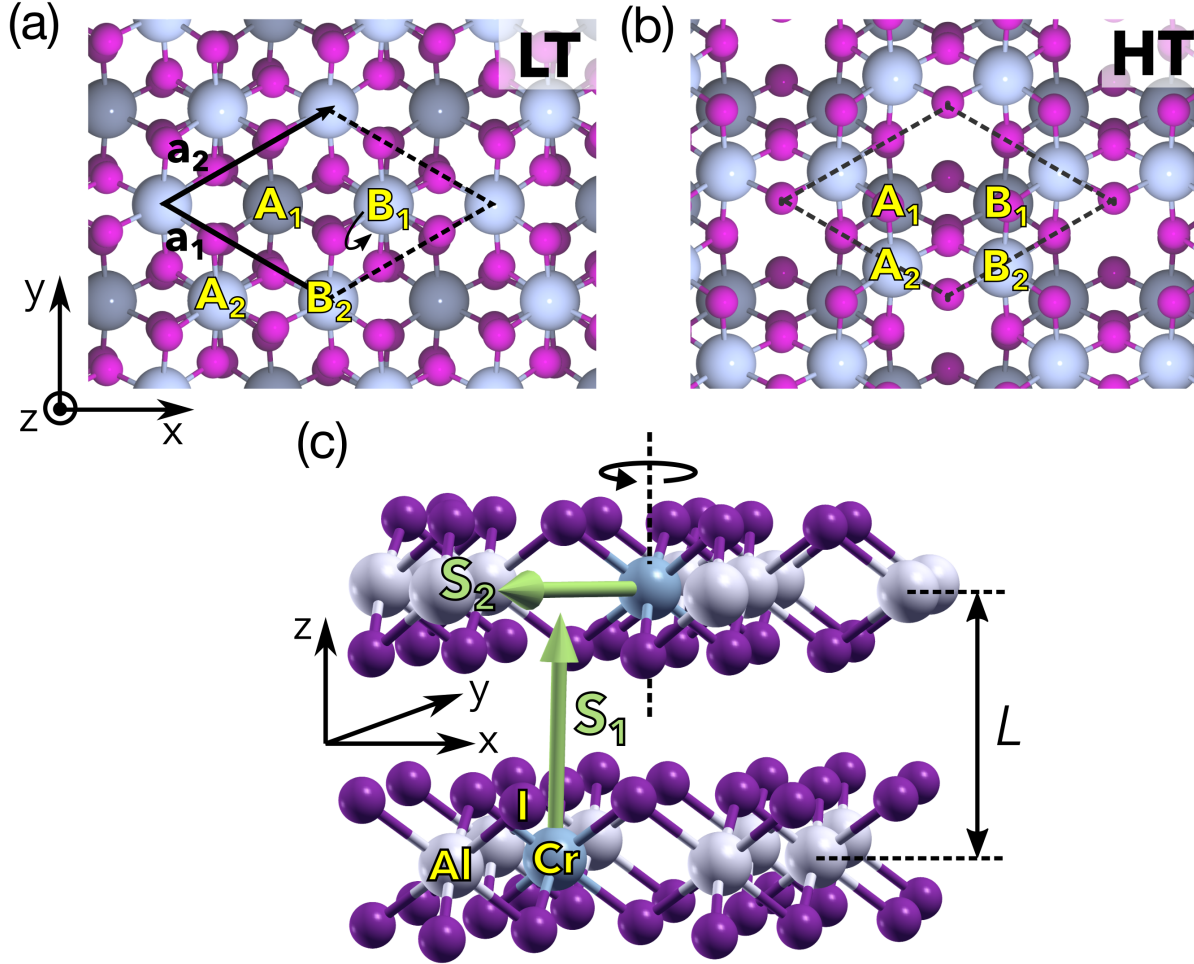


FIG. 1: Bilayer CrI₃ with LT (a) and HT (b) stacking. Atoms from the upper layer are colored by brighter nuances. The HT structure is obtained from LT when the upper layer is translated by $\mathbf{a}_2/3$ (c) One pair of Cr atoms immersed into the CrI₃-like environment with Cr atoms replaced by Al. Spins on Cr atoms are depicted by thick green arrows. The rotation axis is parallel to \mathbf{S}_1 and the spin quantization axis is parallel to \mathbf{S}_2 .

In calculating the interlayer exchange tensors, we follow a two-step computational procedure: in the first step the electron density and the Kohn-Sham wavefunctions are obtained from noncollinear self-consistent field calculations (SCF) without SOC. The directions of spins \mathbf{S}_1 and \mathbf{S}_2 on Cr atoms are constrained perpendicular to one another (Fig. 1c) using the penalty functional⁴². In the second step the Kohn-Sham wavefunctions from the first step are used, the SOC is included on all the atoms and the sum of the band energies are

calculated for different directions of the spin quantization axis. The spin \mathbf{S}_2 is kept parallel to the spin quantization axis so that it rotates together with it, whereas the direction of \mathbf{S}_1 is unaffected by this rotation (see Fig. 1c). Given that only the sum of band energies is used, our procedure can be applied to any system provided that the use of the magnetic force theorem is justified^{43–45}. The benchmark of our method is provided in Supplementary Information, but here we want to stress that our method can save more than 50% of computational time without affecting the accuracy of the reference four-state method^{41,46}.

B. Hamiltonian of two perpendicular spins

Here we derive the model describing the coupling of two perpendicular spins, that is used for mapping the differences between DFT band energies obtained for different directions of the spin quantization axis. In closer detail, we suppose that the two spins belong to different layers, but the model works perfectly fine if spins are from the same layer.

The total energy of such two-spin system is

$$E = E_{\text{nm}} + \mathbf{S}_1 \mathcal{J} \mathbf{S}_2 + \mathbf{S}_1 \mathcal{A}_1 \mathbf{S}_1 + \mathbf{S}_2 \mathcal{A}_2 \mathbf{S}_2, \quad (1)$$

where E_{nm} is the nonmagnetic contribution, \mathcal{J} is an exchange tensor that couples spins \mathbf{S}_1 and \mathbf{S}_2 , and \mathcal{A}_i is the SIA tensor of layer i . If the layers are of the same material and magnetic atoms are Wyckoff partners sharing the same site symmetries, we have $\mathcal{A}_1 = \mathcal{A}_2 = \mathcal{A}$. Without loss of generality let us choose the coordinate system by fixing \mathbf{S}_1 along the z -axis and placing \mathbf{S}_2 in the xy -plane. Now, $\mathbf{S}_1 = (0, 0, S_1)$ and $\mathbf{S}_2 = (S_2 \cos(\phi), S_2 \sin(\phi), 0)$ so that the spin configuration is completely determined by a single parameter – the angle ϕ between the \mathbf{S}_2 and the x -axis. The Eq. 1 turns into

$$\begin{aligned} E(\phi) &= E_C + S_1 S_2 \left(J_{zx} \cos(\phi) + J_{zy} \sin(\phi) \right) + S_2^2 \left(A_- \sin^2(\phi) + A_+ \sin(2\phi) \right) \\ &= E_C + E_J(\phi) + E_A(\phi), \end{aligned} \quad (2)$$

where we introduced the parameters $A_- \equiv A_{yy} - A_{xx}$ and $A_+ \equiv (A_{xy} + A_{yx})/2$ for convenience and $E_C = E_{\text{nm}} + A_{zz} S_1^2 + A_{yy} S_2^2$ comprises all the terms that are ϕ -independent. The important terms for our discussion are the exchange interaction energy $E_J(\phi)$ and the contribution from the single-ion anisotropy $E_A(\phi)$. If we interchange the roles of \mathbf{S}_1 and \mathbf{S}_2 the Eq. 2 yields J_{xz} and J_{yz} . If we further change the rotation axis from z to x we obtain

J_{xy} and J_{yx} (and J_{xz} and J_{zx} that we have already). Therefore, by considering the sets of spin configurations that we denote as $\{\mathbf{S}_1 \parallel z \leftrightarrow \mathbf{S}_2 \circlearrowleft z\}$ and $\{\mathbf{S}_1 \parallel x \leftrightarrow \mathbf{S}_2 \circlearrowleft x\}$, one obtains all the *off-diagonal* \mathcal{J} -matrix elements.

In general, the \mathcal{J} tensor decomposes into the isotropic Heisenberg exchange and the anisotropic DMI (antisymmetric) and KI (symmetric)⁴⁶,

$$\mathcal{J} = \underbrace{\frac{1}{3}\text{Tr}(\mathcal{J})\mathbb{I}_3}_{\text{Heisenberg exchange}} + \underbrace{\frac{1}{2}(\mathcal{J} - \mathcal{J}^T)}_{\text{DMI}} + \underbrace{\left[\frac{1}{2}(\mathcal{J} + \mathcal{J}^T) - \frac{1}{3}\text{Tr}(\mathcal{J})\mathbb{I}_3\right]}_{\text{anisotropic symmetric exchange}} = \frac{1}{3}\text{Tr}(\mathcal{J})\mathbb{I}_3 + \mathcal{D} + \mathcal{K}. \quad (3)$$

By assumption, the spins are perpendicular and the Heisenberg exchange between them vanishes. Thus, the exchange energy contains only the DMI and the KI contributions, $E_J(\phi) = E_{\text{DM}}(\phi) + E_K(\phi)$. The DMI is usually expressed as the mixed vector product, $E_{\text{DM}} = \mathbf{D} \cdot (\mathbf{S}_1 \times \mathbf{S}_2)$, which introduces the *Dzyaloshinskii vector*,

$$\mathbf{D} = (D_x, D_y, D_z) = \frac{1}{2} \left(J_{yz} - J_{zy}, J_{zx} - J_{xz}, J_{xy} - J_{yx} \right). \quad (4)$$

For a system with a well defined symmetry, the direction of \mathbf{D} can be (at least partially) determined with the help of Moriya rules²². In Supplementary Information we derive the Moriya rules in a form that is more suitable for our purposes.

Within $\{\mathbf{S}_1 \parallel z \leftrightarrow \mathbf{S}_2 \circlearrowleft z\}$ spin configurations, the total variation of the Kitaev energy is $\Delta E_K = 2S_1 S_2 (K_{xz}^2 + K_{zy}^2)^{1/2}$. In analogy to DMI, it is convenient to introduce the vector $\mathbf{K} = \frac{1}{2}(J_{yz} + J_{zy}, J_{zx} + J_{xz}, J_{xy} + J_{yx})$ that quantifies the strength of KI by $\Delta E_K/2S_1 S_2 = (K_x^2 + K_y^2)^{1/2}$. Note that in general the matrix \mathcal{K} , unlike \mathcal{D} , contains the diagonal elements as well that are out of reach of this method as their calculation require the (anti)parallel spin configurations. Therefore, strictly speaking for a given reference frame the parameter K quantifies the strength of the off-diagonal part of the Kitaev interaction.

From Eq. 2, we define the SIA constant as $A = \Delta E_A/S^2$, where ΔE_A is the total variation of the SIA energy term $E_A(\phi)$ for the rotation of spin \mathbf{S} around a given axis. It can be easily derived that, for a fixed rotation axis, the energy $E_A(\phi)$ reaches extrema at $\phi_0^\pm = \arcsin\left(\frac{1}{2} \pm \frac{A_\pm}{2\sqrt{A_\pm^2 + 4A_\pm^2}}\right)^{1/2}$ and its total variation is $\Delta E_A = |E(\phi_0) - E(\phi_0 + \pi/2)|$. If spin rotates around the z -axis, the in-plane SIA constant A_\parallel is obtained, whereas if it rotates around the x -(or y -) axis the fitting gives the out-of-plane SIA constant, A_\perp . To sum up all being written about this model, if one performs the DFT calculations for $\{\mathbf{S}_1 \parallel z \leftrightarrow \mathbf{S}_2 \circlearrowleft z\}$ and $\{\mathbf{S}_1 \parallel x \leftrightarrow \mathbf{S}_2 \circlearrowleft x\}$ sets of spin configurations, the \mathbf{D} , \mathbf{K} , A_\perp , and A_\parallel are obtained

from fitting to Eq. 2. We discuss this below for the cases of two Cr atoms from different layers.

C. Interlayer coupling of perpendicular Cr magnetic moments

Bilayer CrI_3 is an illustrative example as it reveals a few different scenarios of interlayer exchange coupling and elucidates the important role of the symmetry of local environment around Cr ions. We will refer to Cr ions pair with its surrounding ligands as “the $\text{CrI}_n\text{-I}_n\text{Cr}$ cluster” (n is the number of ligands that participate in the exchange path between Cr ions). We consider the nearest and the next-nearest interlayer neighbors in both LT and HT structures. The coordinate system is chosen in a way so that the Cr-Cr bond is along the x -axis, while the z -axis is perpendicular to the CrI_3 plane (see Fig. 2a). For each considered structure, we perform the symmetry analysis to double check whether the calculated off-diagonal \mathcal{J} -matrix elements comply with the extended Moriya rules exposed in Supplementary Information.

Starting with the LT bilayer, the nearest and the next-nearest interlayer Cr neighbors are modeled by LT_1 and LT_2 structures (see Fig. 2a-b). In LT_1 the Cr-Cr bond displays inversion, threefold rotation axis parallel to the bond, and three vertical mirror planes. Therefore, the symmetry of $\text{CrI}_3\text{-I}_3\text{Cr}$ cluster in LT_1 satisfies three Moriya rules (a,c,e) and consequently the exchange matrix must be diagonal. In complete agreement our calculations give all the zeros at the off-diagonal slots of the exchange matrix ($\mathcal{J}_{\text{LT}_1}$ in Eq. S1). Moving further to next-nearest neighbors, the $\text{CrI}_2\text{-I}_2\text{Cr}$ cluster in LT_2 has only the spatial-inversion symmetry (Moriya rule a) and the exchange matrix is symmetric, thus forbidding the DMI. On the other hand, no symmetry rule forbids the KI and our calculations reveal $K = 32 \mu\text{eV}$ (Table I). From this example one can actually see the Kitaev interaction in action: with \mathbf{S}_1 fixed along the z -axis and \mathbf{S}_2 rotating around it, the energy of the system is changing according to the *cardioid* pattern which is the direct consequence of the KI (see the polar plot in Fig. 2b).

Moving the discussion to HT stacking, the x -axis is a twofold rotational axis for both $\text{CrI}_2\text{-I}_2\text{Cr}$ in HT_1 and CrI-ICr cluster in HT_2 structure (see Fig. 2c-d). Given that the Cr-Cr bond is perpendicular to x -axis, these two cases fall into the Moriya rule d category. Taking into account the choice of the global coordinate system, the symmetry implies $J_{yx} = -J_{xy}$,

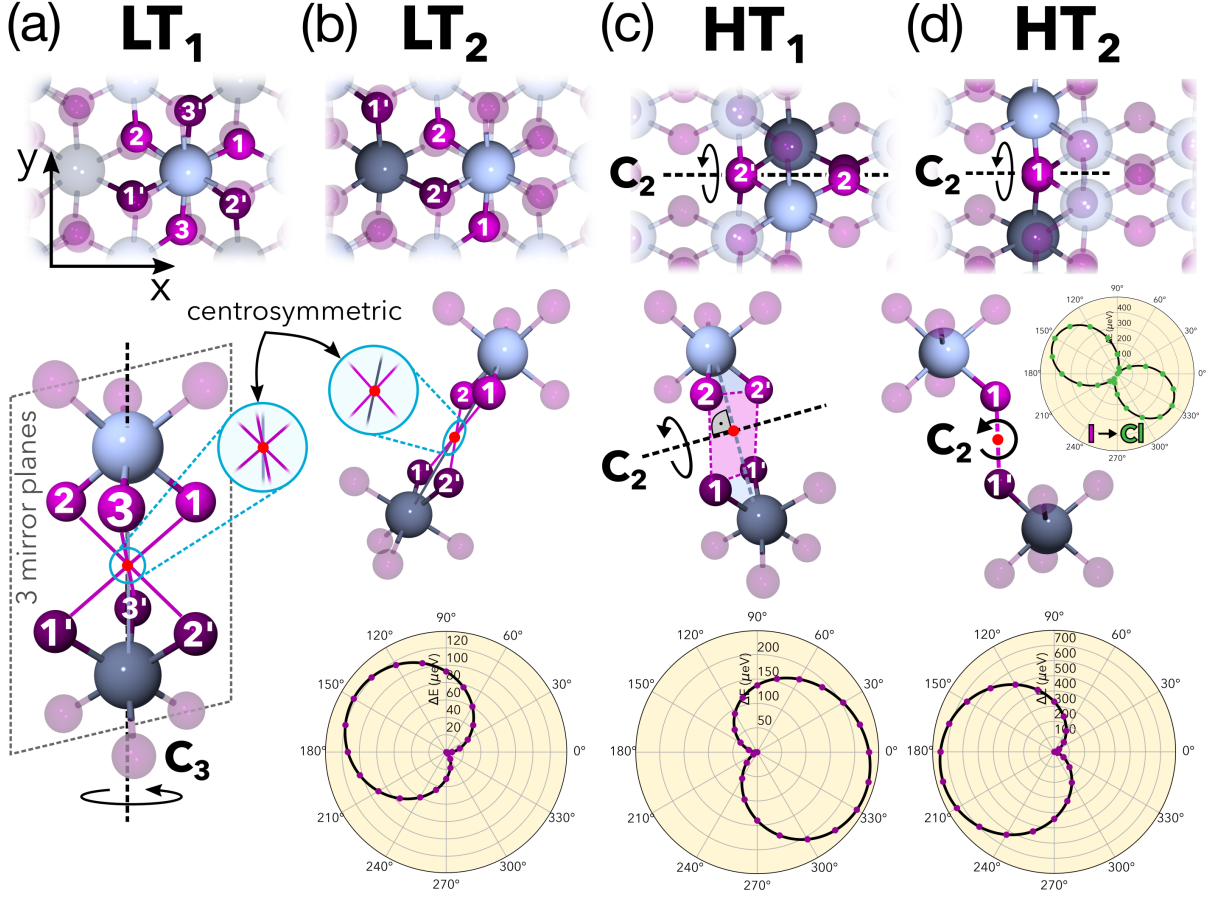


FIG. 2: The structures used for modeling the nearest and the next-nearest interlayer Cr neighbors in LT and HT bilayer (upper panel). The four corresponding $\text{CrI}_n\text{-I}_n\text{Cr}$ clusters are depicted in the middle panel and their symmetries are denoted. Yellow discs show the polar plots of the $E(\phi) - E_0$, where $E(\phi)$ is the sum of band energies for the angle ϕ of the spin quantization axis, and E_0 is the minimum of band energies around the given rotation axis. In d) the ∞ -shaped energy curve corresponds to the HT_2^* structure with I atoms from CrI-ICr cluster replaced by Cl.

$J_{zx} = -J_{xz}$, and $J_{zy} = J_{yz}$. Although KI is not forbidden by symmetry, our calculations reveal its total absence in HT_1 structure and a small K of $25 \mu\text{eV}$ in HT_2 .

Strikingly, both the nearest and the next-nearest interlayer neighbors in HT structure display considerable DMI in the range of $150 - 200 \mu\text{eV}$ (Table I). In Moriya's seminal paper, the DMI is derived from SOC and it is shown that the DM energy is linear in SOC^{22} . Given that the SOC on iodine (and not on chromium) gives the major contribution to MAE of monolayer $\text{CrI}_3^{17,21,47}$, we assume that it is also responsible for the interlayer DMI in bilayer

TABLE I: The magnitude and the components of Dzyaloshinskii and Kitaev vectors. The last two columns present the out-of-plane and the in-plane SIA constants.

structure $ \mu\text{eV} \rightarrow$	$ \mathbf{D} $	D_x	D_y	D_z	$ \mathbf{K} $	K_x	K_y	K_z	A_{\perp}	A_{\parallel}
LT ₁ (Fig. 2a)	0	0	0	0	0	0	0	0	253	0
LT ₂ (Fig. 2b)	0	0	0	0	32	-14	24	-16	240	1
HT ₁ (Fig. 2c)	175	0	50	-168	0	0	0	0	172	19
HT ₂ (Fig. 2d)	166	0	-166	-4	25	-25	0	0	173	12
HT ₂ [*] (CrCl-ClCr)	14	0	-14	3	1	-1	0	0	163	186

CrI₃. This assumption can be tested through ligand replacement. The SOC constant for valence electrons in solids scales as $\lambda \sim 1/Z^2$, where Z is the atomic number⁴⁸. Therefore, if iodines are replaced with chlorine, by the rule of thumb the DMI would be reduced by $Z_{\text{I}}^2/Z_{\text{Cl}}^2 \approx 10$ times. This simple estimate works surprisingly well, as we reveal that the D is reduced 12 times when the two iodines in HT₂ cluster are replaced by chlorine (see Fig. 2d and Table I). Moreover, this example proves the local character of the interlayer DMI, showing that only the ligands in the vicinity of Cr-Cr pair play a role in mediating this anisotropic interaction. Otherwise, the DMI would not be reduced so drastically even after the I \rightarrow Cl replacement in the CrI-ICr cluster because the other iodines are still present in the structure. The dependence of DMI on SOC is further discussed in Subsection II E.

To the best of our knowledge, the effect of stacking on SIA is not addressed in previous studies of bilayer or bulk CrI₃. Most often, it is assumed that the SIA obtained from calculations on the monolayer persists in bilayer and bulk. However, SIA is a local property and is thus sensitive to changes of the spin environment, e.g. by altering the stacking sequence in bilayer. Remarkably, we obtained the increase of 50% in A_{\perp} from HT to LT stacking (Table I). Given that SIA largely contributes to magnetic anisotropy, one must take this change into account when estimating the critical temperature of bilayer or bulk CrI₃. Further, we obtained that LT bilayer is isotropic to the in-plane spin rotations ($A_{\parallel} = 0$) like in the monolayer CrI₃²⁷, but not in HT bilayer where a small in-plane SIA of $A_{\parallel} \sim 10\text{--}20 \mu\text{eV}$ is induced by stacking. This in-plane SIA is responsible for the distortion of the cardioid that corresponds to the HT₁ structure, Fig. 2c. Taking into account all being written in this Section, one should be truly careful in ascribing the monolayer magnetic properties to

bilayer and bulk VdW magnets, as the interlayer interactions proved more important than was initially expected.

D. Interlayer coupling of perpendicular magnetizations

In this Subsection we move away from the two-spin systems and provide the description of coupling between the fully magnetized layers with perpendicular magnetizations. With fully magnetized layers, we assume that all the spins in the layer point to the same direction. In general, when spins are randomly distributed, the total energy of $N \times N$ bilayer CrI_3 (that contains $2N^2$ spins per layer) is a sum of the nonmagnetic energy, the contributions from the *intralayer* and *interlayer* exchange coupling of spins, and SIA contributions at each spin site,

$$E_N = E_{N,\text{nm}} + \sum_{i_1, i_2=1}^{2N^2} \mathbf{S}_{i_1} \mathcal{J}_{i_1 i_2}^\dagger \mathbf{S}_{i_2} + \sum_{l=1,2} \left[\frac{1}{2} \sum_{i_l, j_l=1}^{2N^2} \mathbf{S}_{i_l} \mathcal{J}_{i_l j_l}^{\leftrightarrow} \mathbf{S}_{j_l} + \sum_{i_l=1}^{2N^2} \mathbf{S}_{i_l} \mathcal{A} \mathbf{S}_{i_l} \right], \quad (5)$$

where $l = 1, 2$ is the layer index and i_l and j_l are indices numbering the spin sites. The *interlayer* exchange tensor $\mathcal{J}_{i_1 i_2}^\dagger$ describes the coupling between the spins i_1 and i_2 from different layers, whereas the *intralayer* exchange tensor $\mathcal{J}_{i_l j_l}^{\leftrightarrow}$ describes the coupling between spins i_l and j_l from the same layer l .

If we assume that all the spins belonging to one layer point to the same direction, i.e. $\mathbf{S}_{i_l} \equiv \mathbf{S}_l$, the Eq. 5 greatly simplifies,

$$E = E_{\text{nm}} + \mathbf{S}_1 \left(\underbrace{\mathcal{J}_{A_1 A_2}^\dagger + \mathcal{J}_{A_1 B_2}^\dagger + \mathcal{J}_{B_1 A_2}^\dagger + \mathcal{J}_{B_1 B_2}^\dagger}_{\mathcal{J}^\dagger} \right) \mathbf{S}_2 + \sum_l \mathbf{S}_l \left(\frac{1}{2} \mathcal{J}_A^{\leftrightarrow} + \frac{1}{2} \mathcal{J}_B^{\leftrightarrow} + 2\mathcal{A} \right) \mathbf{S}_l, \quad (6)$$

where $E = E_N/N^2$ and $E_{\text{nm}} = E_{N,\text{nm}}/N^2$ are the total and the non-magnetic energy expressed per unit cell. In Eq. 6 the contributions from A and B sublattices (see Fig. 1a,b) are separated in a sense that $\mathcal{J}_{A_1 B_2}^\dagger$ describes the interlayer coupling between all the spins at A_1 sites with all the spins at B_2 sites (N^2 of each). The tensor $\mathcal{J}_A^{\leftrightarrow}$ describes the interaction of a single spin at A site with all the other spins from the same layer. If we specify the spins $\mathbf{S}_1 = (0, 0, S_1)$ and $\mathbf{S}_2 = (S_2 \cos(\phi), S_2 \sin(\phi), 0)$ the Eq. 6 reads

$$E(\phi) = E_C + S_1 S_2 \left(J_{zx}^\dagger \cos(\phi) + J_{zy}^\dagger \sin(\phi) \right) + S_2^2 \left(Q_- \sin^2(\phi) + Q_+ \sin(2\phi) \right), \quad (7)$$

which is the same equation as Eq. 2. The parameters Q_- and Q_+ stemming from $\mathcal{J}^{\leftrightarrow}$ and

\mathcal{A} will be used solely for fitting purposes and will not be further discussed, as our focus is on \mathcal{J}^\dagger .

We calculated the off-diagonal elements of \mathcal{J}^\dagger -matrix for HT bilayer and obtained a weak interlayer KI of $K = 18 \mu\text{eV}$. On the other hand, already from the spatial-inversion symmetry of HT bilayer we know that there is no DMI as the A_1A_2 (A_1B_2) contribution to the Dzyaloshinskii vector exactly cancels that from B_1B_2 (B_1A_2). Nevertheless, this does not mean that the interlayer DMI between the sublattices is zero. To inspect this, we modeled the A_1A_2 sublattice of the HT structure by replacing the Cr atoms of the B_1B_2 sublattice with Al (Fig. 3a) and obtained the Dzyaloshinskii vector with a magnitude of $D_{A_1A_2} = 236 \mu\text{eV}$. This is a remarkable result, as the estimated $\frac{D}{J}$ ratio is 80% (J from Ref.³¹), much higher than the 10% threshold which is already considered promising for skyrmionics⁴⁹⁻⁵¹. Compared with the experimental results, the $D_{A_1A_2}$ is twice higher than the interlayer DM energy reported for TbFe/Pt/Co multilayers, which is among the strongest interlayer DMI realized in experiments⁴⁰.

E. Dependence of DMI/KI on structural transformations and SOC

As shown in Fig. 3b, the magnitude of both the DMI and KI display a fast, exponential-like decrease when the interlayer distance L is larger than $\approx 3 \text{ \AA}$, consistently with the expected weak interaction between the layers across the VdW gap. At shorter separation, the evolution with L suggests a more complicated situation, especially for the KI which displays a non-monotonic behavior. Assuming a superexchange-like mechanism for both interactions, the dependence on the interlayer distance can be rationalized taking into account the possible exchange paths involving different transfer integrals (hopping terms) between Cr and I ions and their expected dependence on the relative bond lengths l . One can identify three such hopping terms, corresponding to $d_{Cr}-d_{Cr}$ direct hopping ($t_1 \propto l^{-5}$), $d_{Cr}-p_I$ hopping ($t_2 \propto l^{-7/2}$) and p_I-p_I hopping ($t_3 \propto l^{-2}$), where we adopted the bond-length dependence of Harrison⁵². In perturbation theory, the exchange interaction can be expressed quite generally as a sum of terms each with the form $t^n F(\lambda, U, \Delta)$, where $F(\lambda, U, \Delta)$ is a polynomial function of atomic SOC λ , charge transfer energy Δ , and on-site Coulomb interaction U and the exponent n depends on the number of hopping terms involved in the exchange path. For instance, the contribution to the exchange interaction arising from the direct $d-d$ hopping

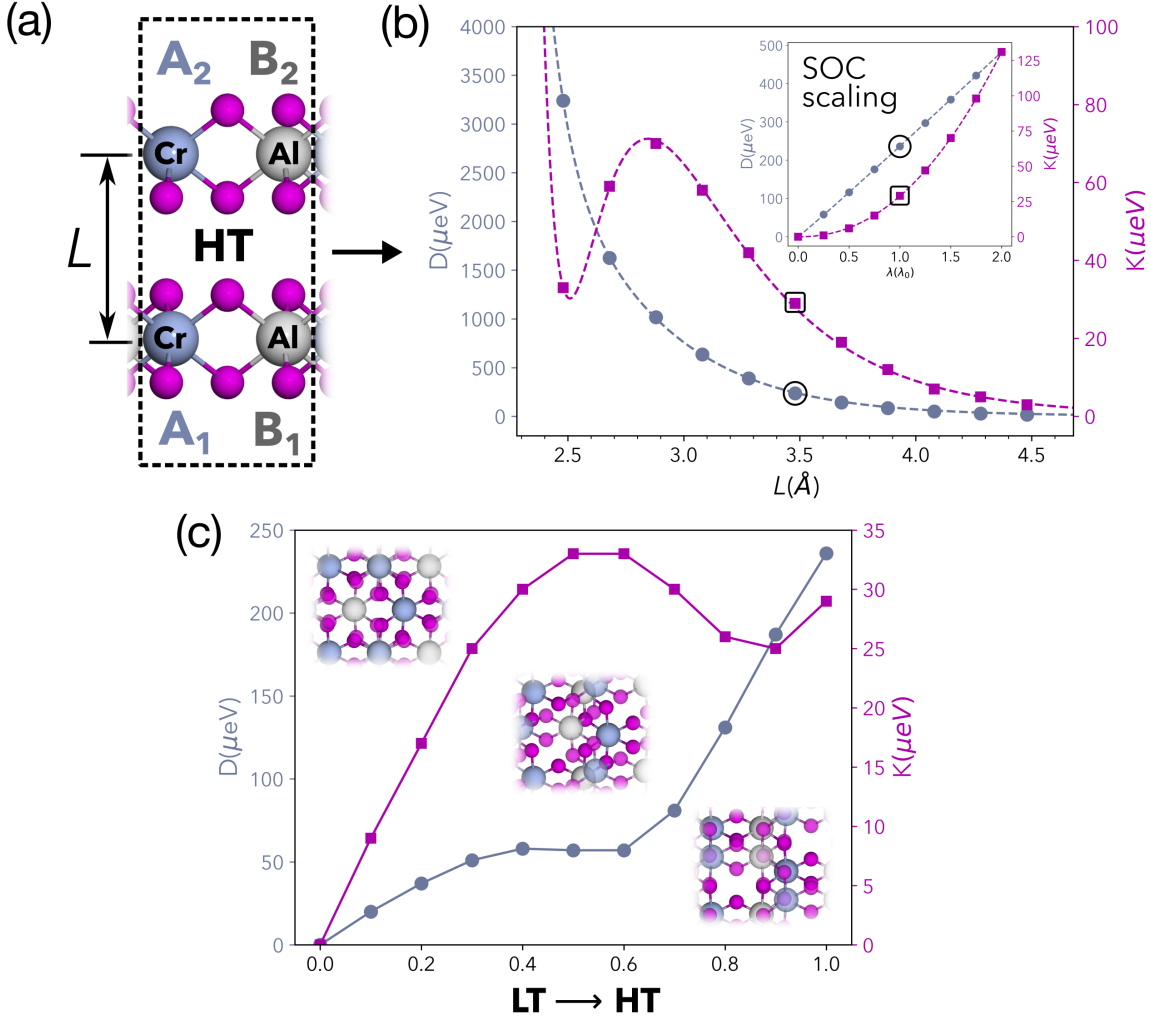


FIG. 3: (a) Magnitudes of the Dzyaloshinskii (D) and Kitaev (K) vectors as a function of interlayer distance for A_1A_2 sublattice of HT structure. Dashed lines are fitted lines with parameters $c_{10}^D = 95 \text{ eV}\text{\AA}^{-10}$, $c_{10}^K = 13 \text{ eV}\text{\AA}^{-10}$, $c_{14}^D = -5.46 \times 10^3 \text{ eV}\text{\AA}^{-14}$, $c_{10}^K = -0.98 \times 10^3 \text{ eV}\text{\AA}^{-14}$, $c_{18}^D = 1.11 \times 10^5 \text{ eV}\text{\AA}^{-18}$ and $c_{18}^K = 0.19 \times 10^5 \text{ eV}\text{\AA}^{-18}$. In the inset the D and K dependence on SOC constant is depicted as calculated for $L = 3.48 \text{ \AA}$ (dashed lines displaying the fitting power function discussed in the text). (b) The D and K dependence on the stacking sequence from LT to HT structure for $L = 3.48 \text{ \AA}$. Continuous lines are guides for the eye.

between Cr atoms scales as $t_1^2 \propto l^{-10} \sim L^{-10}$. Similarly, a Cr-I-Cr exchange path involving a single ligand I- p intermediate state would scale as $t_2^4 \sim L^{-14}$, while a Cr-I-I-Cr exchange path would also include a p - p transfer integral, scaling overall as $t_2^4 t_3^2 \sim L^{-18}$. Neglecting the details of the bond geometries and the angular dependence of each transfer integral and

assuming that the dependence on the interlayer distance inherits the same scaling law of hopping terms, one can derive a general functional expression for both D and K that reads

$$I(L) = \frac{c_{10}^I}{L^{10}} + \frac{c_{14}^I}{L^{14}} + \frac{c_{18}^I}{L^{18}}, \quad (8)$$

where I stands for D or K and c_n^I are fitting parameters effectively including all the complicated dependence on interaction matrix elements. We stress the fact that different exchange paths can give rise to perturbation terms with the same scaling dependence on the interlayer distance, that are effectively regrouped in Eq. 8. As an example, the Cr-I-Cr exchange path shares the same L^{-14} dependence with a process where an electron is transferred from one Cr- d to the other magnetic atom through both ligands and then transferred back via a direct d - d process.

Despite the underlying crude approximations, Eq. 8 captures surprisingly well the evolution of both DMI and KI as a function of the overall interlayer distance, as shown in Fig. 3b. Remarkably, the non-monotonic dependence of KI can be quite naturally interpreted as arising from the competition of different super-superexchange processes occurring across the VdW gap. Notwithstanding the phenomenological nature of the fitting parameters, some general trends can be deduced. For both interaction terms, c_{14}^I is negative while c_{10}^I and c_{18}^I are positive: the largest coefficients are those involving p - p hopping terms, which dominate at short separation, while in the opposite limit the first term – showing a slower decay – prevails. For instance, at the optimal distance $L_{\text{opt}} = 3.48 \text{ \AA}$, one has $D(L_{\text{opt}}) = (366 - 143 + 20) \mu\text{eV}$ and $K(L_{\text{opt}}) = (50 - 25 + 3) \mu\text{eV}$, with the dominant contribution arising from the slow-decaying $c_{10}^I L^{-10}$ term: a compression of 18% causes an increase of both interactions by more than 300% and 140%, respectively, but the first two terms in Eq. 8 largely compensate each other and the third term starts to kick in, as $D(0.82L_{\text{opt}}) = (2.66 - 2.30 + 0.70) \text{ meV}$ and $K(0.82L_{\text{opt}}) = (0.36 - 0.41 + 0.12) \text{ meV}$.

It is worth reminding that the intralayer Kitaev interaction in monolayer CrI_3 (not to be confused with K as defined in Subsection II B) has been shown to scale quadratically with ligand iodine SOC, the transition-metal SOC contribution being negligible²¹. The superexchange mechanisms leading to anisotropic exchange interactions are therefore different from those discussed in the seminal Moriya's paper²², where it was assumed that the spin of the magnetic atom couples to its own orbital moment. On the other hand, the microscopic mechanisms at play are analogous to those analysed for related transition-metal dihalides, sharing

with trihalides similar local bonding environments and strong magnetic anisotropies^{53,54}. To shed light on SOC dependence of interlayer anisotropic exchange couplings in bilayer CrI₃, we varied the SOC constant from $\lambda = 0$ (no SOC) to $\lambda = 2\lambda_0$ (double the original value), as shown in the inset of Fig. 3b, and fitted the values to the power function $g(\lambda) = g_0\lambda^n$. The fit yielded $n_D = 1.03$ and $n_K = 2.19$ (see Fig. 3c), meaning that D is a linear function of λ whereas K has nearly quadratic behavior as the intralayer Kitaev interaction. The scaling analysis on both SOC and interlayer distance suggests that superexchange mechanisms are effective in CrI₃ bilayer despite the presence of a VdW gap.

To examine the influence of a stacking sequence we gradually translated the upper layer along the \mathbf{a}_2 lattice vector, starting from the LT and ending with the HT structure (Fig. 3c). The different behavior of D and K with stacking alteration demonstrates the importance of angles in the Cr-I-I-Cr bonds for hopping processes that are governing the interlayer interaction. Along the inspected direction of translation, K reaches its maximum of $33 \mu\text{eV}$ on the halfway between the LT and HT, whereas the maximum of D of $236 \mu\text{eV}$ is in the HT structure. It is interesting to see that for structures that are intermediate between LT and HT the DMI and KI are the same order of magnitude. Note that in order to find the global maximum of D and K one should inspect all possible directions, which is a demanding computational task that goes out of the scope of the present work.

III. DISCUSSION

DFT calculations supported by Hamiltonian modeling reveal strong interlayer DMI in A_1A_2 (B_1B_2) sublattice of HT bilayer CrI₃. At the microscopic scale, DMI in HT bilayer emerges between the nearest and the next-nearest interlayer Cr neighbors due to broken local spatial inversion. However, due to the global C_2 symmetry of sublattices, the contributions from A_1A_2 and B_1B_2 cancel each other resulting in zero net macroscopic DMI. In addition to DMI, there is an order of magnitude weaker interlayer KI that does not vanish due to symmetry. In LT structure there is no DMI as the Cr-Cr pair with their surrounding iodines are centrosymmetric. Despite the DMI in HT structure dies out at the macroscopic scale, the main result of this work is the demonstration of the ability of iodine ligands to efficiently mediate the anisotropic exchange between the magnetic layers. This ability comes from the strong SOC of spatially extended I-5*p* orbitals and is impaired if iodine atoms are replaced

by other ligands that have weaker SOC. The developed computational procedure offers unprecedented accuracy in calculating the anisotropic exchange interactions. Being quite general, it can be applied in any magnetic material provided that the use of the magnetic force theorem is physically sound. The symmetry analysis and the benchmark with the reference four-state method firmly support the accuracy offered by our method. In addition to the detailed analysis of the anisotropic interlayer exchange, we demonstrated that SIA heavily depends on stacking. Therefore, in estimating the Curie temperature of bilayer or bulk VdW magnet, one should not use the SIA calculated for a monolayer but instead should calculate the SIA for the system of interest.

With all being said, bilayer CrI_3 is not an appropriate 2D magnetic system for the experimental demonstration of interlayer DMI. Notwithstanding, we identified all the bricks needed to build one. Instead of attempting to modify the bilayer CrI_3 , the approach that seems more promising is to build from scratch a new heterostructure by finding an appropriate 2D magnet that can complement a layer of CrI_3 . Using a different 2D magnet as second layer has a huge advantage in inducing DMI, as one doesn't need to worry about the spatial-inversion symmetry which is trivially broken by different chemical composition of the two layers. To efficiently mediate the DMI between the magnetic ions, a candidate 2D magnet should have ligands that feature strong SOC. Most importantly, contrary to CrI_3 it should show in-plane magnetic anisotropy in order to maximize the $|\mathbf{M}_1 \times \mathbf{M}_2|$ product and its MAE should be strong enough to compete with the interlayer Heisenberg exchange that favors the (anti)parallel spin configuration.

Within the CrX_3 family of 2D magnets only CrCl_3 shows an easy-plane MAE²⁷, but the other properties discredit it from potential candidacy. First, its MAE is extremely small and when combined with CrI_3 all the chances are that the interlayer Heisenberg exchange will prevail, directing CrCl_3 magnetization out of plane. Second, the Cr-I-Cl-Cr interaction path is far less efficient than Cr-I-I-Cr in mediating DMI, due to small SOC on Cl. We further note that due to the lattice constant mismatch between CrI_3 and CrCl_3 one would need to match 6×6 structure of CrI_3 with 7×7 structure of CrCl_3 to build a $\text{CrI}_3/\text{CrCl}_3$ heterostructure, ending up with a 680 atoms in the supercell. Hence, due to high computational demands, we were not able to check these assumptions, thus leaving the search for a potential candidate for future studies.

IV. METHODS

DFT calculations are performed using the VASP code⁵⁵. To describe the effects of electronic exchange and correlation we used the Perdew–Burke–Ernzerhof (PBE) functional⁵⁶. We did not employ an effective Hubbard parameter U but we are aware that the choice of U may affect the exchange coupling, as it is the case for monolayer CrI_3 ²¹. The lattice constant $a = 7.005 \text{ \AA}$ of monolayer CrI_3 is obtained from spin-polarized collinear DFT calculations assuming the FM ground state. The interlayer distance is set to $L_{\text{opt}} = 3.48 \text{ \AA}$, which corresponds to the experimental interlayer distance in bulk HT structure²⁹. The bilayer made by stacking two monolayers was not relaxed any further. The lattice vector along the c -axis was set to 30 \AA so that the vacuum between periodic replicas along c -axis is 20 \AA thick. A cutoff of 450 eV is imposed onto the plane wave basis set and the total energies are converged to the precision of $10^{-9} \text{ eV/electron}$. The Brillouin zone of the $2 \times 2 (3 \times 3)$ supercell was sampled by Γ -centered $4 \times 4 \times 1 (3 \times 3 \times 1)$ k -points mesh. The results didn't change with further increase in k -point density owing to semiconducting nature of CrI_3 . The directions of magnetic moments on Cr atoms were constrained using the approach exposed in Ref.⁴². We carefully checked whether the size of the sphere (RWIGS) used for calculating the magnetic moments on Cr atoms and the weight of the penalty functional (LAMBDA) affect the obtained \mathcal{J} -matrix elements. In the end we used $\text{RWIGS} = 1.323 \text{ \AA}$ and $\text{LAMBDA} = 10$.

Acknowledgment

The authors acknowledge support from the Italian Ministry for Research and Education through PRIN-2017 projects “TWEET: Towards ferroelectricity in two dimensions” (IT-MIUR Grant No. 2017YCTB59) and “Quantum 2D: Tuning and understanding Quantum phases in 2D materials” (IT-MIUR Grant No. 2017Z8TS5B). SS thanks Marko Milivojević for very useful discussions about the role of spin-orbit coupling in the superexchange interaction.

References

- * Electronic address: srdjan.stavric@spin.cnr.it
- ¹ Huang, B. *et al.* Layer-dependent ferromagnetism in a van der Waals crystal down to the monolayer limit. *Nature* **546**, 270–273 (2017).
 - ² Gong, C. *et al.* Discovery of intrinsic ferromagnetism in two-dimensional van der Waals crystals. *Nature* **546**, 265–269 (2017).
 - ³ Klein, D. R. *et al.* Probing magnetism in 2D van der Waals crystalline insulators via electron tunneling. *Science* **360**, 1218–1222 (2018).
 - ⁴ Song, T. *et al.* Giant tunneling magnetoresistance in spin-filter van der Waals heterostructures. *Science* **360**, 1214–1218 (2018).
 - ⁵ Wang, Z. *et al.* Very large tunneling magnetoresistance in layered magnetic semiconductor CrI₃. *Nat. Commun.* **9**, 1–8 (2018).
 - ⁶ Gibertini, M., Koperski, M., Morpurgo, A. F. & Novoselov, K. S. Magnetic 2D materials and heterostructures. *Nat. Nanotechnol.* **14**, 408–419 (2019).
 - ⁷ Soriano, D., Katsnelson, M. I. & Fernández-Rossier, J. Magnetic Two-Dimensional Chromium Trihalides: A Theoretical Perspective. *Nano Lett.* **20**, 6225–6234 (2020).
 - ⁸ Huang, B. *et al.* Electrical control of 2D magnetism in bilayer CrI₃. *Nat. Nanotechnol.* **13**, 544–548 (2018).
 - ⁹ Morell, E. S., León, A., Miwa, R. H. & Vargas, P. Control of magnetism in bilayer CrI₃ by an external electric field. *2D Mater.* **6**, 025020 (2019).
 - ¹⁰ Jiang, P. *et al.* Stacking tunable interlayer magnetism in bilayer CrI₃. *Phys. Rev. B* **99**, 144401 (2019).
 - ¹¹ Song, T. *et al.* Switching 2D magnetic states via pressure tuning of layer stacking. *Nat. Mater.* **18**, 1298–1302 (2019).
 - ¹² Xu, Y. *et al.* Coexisting ferromagnetic–antiferromagnetic state in twisted bilayer CrI₃. *Nat. Nanotechnol.* **17**, 143–147 (2022).
 - ¹³ Dolui, K. *et al.* Proximity Spin–Orbit Torque on a Two-Dimensional Magnet within van der Waals Heterostructure: Current-Driven Antiferromagnet-to-Ferromagnet Reversible Nonequi-

- librium Phase Transition in Bilayer CrI₃. *Nano Lett.* (2020).
- ¹⁴ Zhang, Y. *et al.* Switchable magnetic bulk photovoltaic effect in the two-dimensional magnet CrI₃. *Nat. Commun.* **10**, 1–7 (2019).
- ¹⁵ Soriano, D. & Katsnelson, M. I. Magnetic polaron and antiferromagnetic-ferromagnetic transition in doped bilayer CrI₃. *Phys. Rev. B* **101**, 041402 (2020).
- ¹⁶ Lei, C. *et al.* Magnetoelectric Response of Antiferromagnetic CrI₃ Bilayers. *Nano Lett.* **21**, 1948–1954 (2021).
- ¹⁷ Lado, J. L. & Fernández-Rossier, J. On the origin of magnetic anisotropy in two dimensional CrI₃. *2D Mater.* **4**, 035002 (2017).
- ¹⁸ Besbes, O., Nikolaev, S., Meskini, N. & Solovyev, I. Microscopic origin of ferromagnetism in the trihalides CrCl₃ and CrI₃. *Phys. Rev. B* **99**, 104432 (2019).
- ¹⁹ Kashin, I. V., Mazurenko, V. V., Katsnelson, M. I. & Rudenko, A. N. Orbitally-resolved ferromagnetism of monolayer CrI₃. *2D Mater.* **7**, 025036 (2020).
- ²⁰ Mermin, N. Crystalline Order in Two Dimensions. *Phys. Rev.* **176**, 250–254 (1968).
- ²¹ Xu, C., Feng, J., Xiang, H. & Bellaiche, L. Interplay between Kitaev interaction and single ion anisotropy in ferromagnetic CrI₃ and CrGeTe₃ monolayers. *npj Comput. Mater.* **4**, 1–6 (2018).
- ²² Moriya, T. Anisotropic Superexchange Interaction and Weak Ferromagnetism. *Phys. Rev.* **120**, 91–98 (1960).
- ²³ Evans, R. F. L., Rózsa, L., Jenkins, S. & Atxitia, U. Temperature scaling of two-ion anisotropy in pure and mixed anisotropy systems. *Phys. Rev. B* **102**, 020412 (2020).
- ²⁴ Webster, L. & Yan, J.-A. Strain-tunable magnetic anisotropy in monolayer CrCl₃, CrBr₃, and CrI₃. *Phys. Rev. B* **98**, 144411 (2018).
- ²⁵ Lu, X., Fei, R. & Yang, L. Curie temperature of emerging two-dimensional magnetic structures. *Phys. Rev. B* **100**, 205409 (2019).
- ²⁶ Xue, F., Hou, Y., Wang, Z. & Wu, R. Two-dimensional ferromagnetic van der Waals CrCl₃ monolayer with enhanced anisotropy and Curie temperature. *Phys. Rev. B* **100**, 224429 (2019).
- ²⁷ Lu, X., Fei, R., Zhu, L. & Yang, L. Meron-like topological spin defects in monolayer CrCl₃. *Nat. Commun.* **11**, 1–8 (2020).
- ²⁸ Jaeschke-Ubiergo, R., Suárez Morell, E. & Nunez, A. S. Theory of magnetism in the van der Waals magnet CrI₃. *Phys. Rev. B* **103**, 174410 (2021).
- ²⁹ McGuire, M. A., Dixit, H., Cooper, V. R. & Sales, B. C. Coupling of Crystal Structure and

- Magnetism in the Layered, Ferromagnetic Insulator CrI₃. *Chem. Mater.* **27**, 612–620 (2015).
- ³⁰ Sivadas, N., Okamoto, S., Xu, X., Fennie, Craig. J. & Xiao, D. Stacking-Dependent Magnetism in Bilayer CrI₃. *Nano Lett.* **18**, 7658–7664 (2018).
- ³¹ Jang, S. W., Jeong, M. Y., Yoon, H., Ryee, S. & Han, M. J. Microscopic understanding of magnetic interactions in bilayer CrI₃. *Phys. Rev. Mater.* **3**, 031001 (2019).
- ³² Soriano, D., Cardoso, C. & Fernández-Rossier, J. Interplay between interlayer exchange and stacking in CrI₃ bilayers. *Solid State Commun.* **299**, 113662 (2019).
- ³³ Kong, X., Yoon, H., Han, M. J. & Liang, L. Switching interlayer magnetic order in bilayer CrI₃ by stacking reversal. *Nanoscale* **13**, 16172–16181 (2021).
- ³⁴ Li, T. *et al.* Pressure-controlled interlayer magnetism in atomically thin CrI₃. *Nat. Mater.* **18**, 1303–1308 (2019).
- ³⁵ Ke, L. & Katsnelson, M. I. Electron correlation effects on exchange interactions and spin excitations in 2D van der Waals materials. *npj Comput. Mater.* **7**, 1–8 (2021).
- ³⁶ Song, K. W. & Fal'ko, V. I. Superexchange and spin-orbit coupling in monolayer and bilayer chromium trihalides. *Phys. Rev. B* **106**, 245111 (2022).
- ³⁷ Akram, M. *et al.* Moiré Skyrmions and Chiral Magnetic Phases in Twisted CrX₃ (X = I, Br, and Cl) Bilayers. *Nano Lett.* **21**, 6633–6639 (2021).
- ³⁸ Yang, B., Li, Y., Xiang, H., Lin, H. & Huang, B. Moiré magnetic exchange interactions in twisted magnets. *Nat. Comput. Sci.* **3**, 314–320 (2023).
- ³⁹ Vedmedenko, E. Y., Riego, P., Arregi, J. A. & Berger, A. Interlayer Dzyaloshinskii-Moriya Interactions. *Phys. Rev. Lett.* **122**, 257202 (2019).
- ⁴⁰ Avci, C. O., Lambert, C.-H., Sala, G. & Gambardella, P. Chiral Coupling between Magnetic Layers with Orthogonal Magnetization. *Phys. Rev. Lett.* **127**, 167202 (2021).
- ⁴¹ Xiang, H., Lee, C., Koo, H.-J., Gong, X. & Whangbo, M.-H. Magnetic properties and energy-mapping analysis. *Dalton Trans.* **42**, 823–853 (2012).
- ⁴² Ma, P.-W. & Dudarev, S. L. Constrained density functional for noncollinear magnetism. *Phys. Rev. B* **91**, 054420 (2015).
- ⁴³ Liechtenstein, A. I., Katsnelson, M. I., Antropov, V. P. & Gubanov, V. A. Local spin density functional approach to the theory of exchange interactions in ferromagnetic metals and alloys. *J. Magn. Magn. Mater.* **67**, 65–74 (1987).
- ⁴⁴ Solovyev, I. V. Exchange interactions and magnetic force theorem. *Phys. Rev. B* **103**, 104428

- (2021).
- ⁴⁵ Soriano, D., Rudenko, A. N., Katsnelson, M. I. & Rösner, M. Environmental screening and ligand-field effects to magnetism in CrI₃ monolayer. *npj Comput. Mater.* **7**, 1–10 (2021).
- ⁴⁶ Li, X. *et al.* Spin Hamiltonians in Magnets: Theories and Computations. *Molecules* **26**, 803 (2021).
- ⁴⁷ Kim, J. *et al.* Exploitable Magnetic Anisotropy of the Two-Dimensional Magnet CrI₃. *Nano Lett.* **20**, 929–935 (2020).
- ⁴⁸ Shanavas, K. V., Popović, Z. S. & Satpathy, S. Theoretical model for Rashba spin-orbit interaction in *d* electrons. *Phys. Rev. B* **90**, 165108 (2014).
- ⁴⁹ Koshibae, W. & Nagaosa, N. Creation of skyrmions and antiskyrmions by local heating. *Nat. Commun.* **5**, 1–11 (2014).
- ⁵⁰ Zhang, Y. *et al.* Emergence of skyrmionium in a two-dimensional CrGe(Se, Te)₃ Janus monolayer. *Phys. Rev. B* **102**, 241107 (2020).
- ⁵¹ Xu, C. *et al.* Topological spin texture in Janus monolayers of the chromium trihalides Cr(I, X)₃. *Phys. Rev. B* **101**, 060404 (2020).
- ⁵² Harrison, W. A. *Electronic Structure and the Properties of Solids* (Dover Publications, N. Y., 1989).
- ⁵³ Amoroso, D., Barone, P. & Picozzi, S. Spontaneous skyrmionic lattice from anisotropic symmetric exchange in a ni-halide monolayer. *Nat. Commun.* **11**, 5784 (2020).
- ⁵⁴ Riedl, K. *et al.* Microscopic origin of magnetism in monolayer 3*d* transition metal dihalides. *Phys. Rev. B* **106**, 035156 (2022).
- ⁵⁵ Kresse, G. & Furthmüller, J. Efficient iterative schemes for ab initio total-energy calculations using a plane-wave basis set. *Phys. Rev. B* **54**, 11169–11186 (1996).
- ⁵⁶ Perdew, J., Burke, K. & Ernzerhof, M. Generalized gradient approximation made simple. *Phys. Rev. Lett.* **77**, 3865–3868 (1996).

SUPPLEMENTARY INFORMATION

Delving into the anisotropic interlayer exchange in bilayer CrI₃

(Dated: May 26, 2023)

I. BENCHMARK OF THE COMPUTATIONAL METHOD

Here we present the benchmark of our method of rotating perpendicular spins and compare it to the reference four-state method. We stress that our method largely reduces the number of SCF calculations that are needed for obtaining the off-diagonal \mathcal{J} -matrix elements. The reason is that, once the electron density is well converged in a noncollinear SCF calculation, the non-SCF calculations for different directions of the spin quantization don't cost much, as each of them takes just a few more iterations. Note that the noncollinear SCF calculations are in general tricky and one should take the opportunity to avoid performing them whenever possible. To demonstrate how much time is saved without loss in accuracy, we calculated the \mathcal{J}_1 -matrix and SIA of monolayer CrI₃. We used the computational parameters reported in the Methods of the Main Text. The calculations were performed using the OpenACC GPU port of VASP 6.3.2 on a single node equipped with 4 NVIDIA Volta V100 GPUs and 256 GB of RAM. The results summarized in Table S1 show that our method can halve the computational time.

TABLE S1: Out-of-plane SIA (A_\perp) and matrix elements of \mathcal{J}_1 obtained with the reference four-state method and with our method. As our method doesn't provide the diagonal matrix elements, in accounting the CPU time spent with four-state method we present only the time spent for calculating the off-diagonal matrix elements.

method	A_\perp (μeV)	CPU time(s)	\mathcal{J}_1 (μeV)			CPU time(s)
four-state	297	5284	-3299	-6	0	34681
			3	-2382	389	
			0	390	-2743	
our method	265	1878	***	0	0	16554
		35%	0	***	420	
		48%	0	420	***	

II. EXTENDED MORIYA'S RULES

Here we extend the well-known Moriya's rules, originally devised to deduce the allowed direction of the Dzyaloshinskii vector \mathbf{D} from the crystal symmetry, to the full anisotropic part of the exchange tensor, including both the antisymmetric and the symmetric components. In his seminal paper Ref. 1, Moriya derived five rules for the bilinear exchange coupling between two ions located at points A and B , where the point bisecting the straight line AB (i.e., the bond vector) is denoted by C . Five classes of symmetry were considered, namely:

- inversion center at C
- mirror plane perpendicular to AB and passing through C
- mirror plane including A and B
- two-fold rotation axis perpendicular to AB and passing through C
- n -fold rotation axis ($n \geq 2$) parallel to AB

Each of the considered bond symmetries must leave invariant the following interaction term

$$H_{AB} = \mathbf{S}_A \cdot \mathcal{J}^{AB} \cdot \mathbf{S}_B \equiv \sum_{\alpha\beta} \mathcal{J}_{\alpha\beta}^{AB} S_{A,\alpha} S_{B,\beta} \quad (\text{S1})$$

where α, β denote cartesian components. We choose a cartesian coordinate system where the x axis is parallel to the bond AB , and we denote the five symmetry classes above as i (case a), m_{100} (case b), m_{001} or m_{010} (case c), C_{2z} or

	i	m_{100}	m_{001}	C_{2z}	C_{2x}
$S_{A,x}$	$S_{B,x}$	$S_{B,x}$	$-S_{A,x}$	$-S_{B,x}$	$S_{A,x}$
$S_{A,y}$	$S_{B,y}$	$-S_{B,y}$	$-S_{A,y}$	$-S_{B,y}$	$-S_{A,y}$
$S_{A,z}$	$S_{B,z}$	$-S_{B,z}$	$S_{A,z}$	$S_{B,z}$	$-S_{A,z}$
$S_{B,x}$	$S_{A,x}$	$S_{A,x}$	$-S_{B,x}$	$-S_{A,x}$	$S_{B,x}$
$S_{B,y}$	$S_{A,y}$	$-S_{A,y}$	$-S_{B,y}$	$-S_{A,y}$	$-S_{B,y}$
$S_{B,z}$	$S_{A,z}$	$-S_{A,z}$	$S_{B,z}$	$S_{A,z}$	$-S_{B,z}$

TABLE S2: Transformation table for axial vectors $\mathbf{S}_A, \mathbf{S}_B$ located at points A and B under point-group symmetries for the fixed point C bisecting the straight line AB . For cases c and d we choose m_{001} and C_{2z} symmetry elements without loss of generality (equivalent subcases can be obtained by rotating the reference frame around the x axis). For case e , we take $n = 2$ for the sake of simplicity, but the result can be easily generalized.

C_{2y} (case d) and C_{nx} (case e). The transformation table for the cartesian components of the axial vectors $\mathbf{S}_A, \mathbf{S}_B$ is given as Table S2. We notice that inversion simply acts on the site indices, swapping A and B spins, while m_{001} (or m_{010}) and C_{nx} act on cartesian components without swapping site indices. We focus only on symmetry constraints for off-diagonal components of the tensor \mathcal{J}^{AB} . Indeed, each diagonal component $\mathcal{J}_{\alpha\alpha}^{AB}$ always complies with the considered symmetries, as these do not mix cartesian components, as clearly seen from Table S2.

a. Inversion center at C . Applying the transformation rules of Table S2, it is found that $S_{A,\alpha}S_{B,\beta} \mapsto S_{B,\alpha}S_{A,\beta}$. It follows that, to keep the interaction term invariant, $\mathcal{J}_{\alpha\beta}^{AB} = \mathcal{J}_{\beta\alpha}^{AB}$. Consistently with the first Moriya's rule, the antisymmetric component (i.e., the DMI) must vanish in the presence of inversion symmetry, and the anisotropic part of the full exchange tensor must be symmetric, with no further constraints on off-diagonal components of the pseudo-dipolar term. Using the Dzyaloshinskii vector and the analogous vector \mathbf{K} we introduced to denote the off-diagonal components of the symmetric anisotropic tensor, inversion implies that $\mathbf{D} = 0$ but $\mathbf{K} \neq 0$.

b. Mirror plane perpendicular to AB and passing through C . In this case one finds:

$$\begin{aligned} S_{A,x}S_{B,y} &\mapsto -S_{B,x}S_{A,y}, \\ S_{A,x}S_{B,z} &\mapsto -S_{B,x}S_{A,z}, \\ S_{A,y}S_{B,z} &\mapsto +S_{B,y}S_{A,z}, \end{aligned}$$

implying $\mathcal{J}_{xy}^{AB} = -\mathcal{J}_{yx}^{AB}$, $\mathcal{J}_{xz}^{AB} = -\mathcal{J}_{zx}^{AB}$ and $\mathcal{J}_{yz}^{AB} = +\mathcal{J}_{zy}^{AB}$. The mirror symmetry implies that two purely antisymmetric components exist, corresponding to a Dzyaloshinskii vector \mathbf{D} perpendicular to the AB (x) axis, or equivalently lying in the mirror plane, as stated by the second Moriya's rule. Additionally, there is a purely symmetric part of the anisotropic exchange tensor coupling spin components lying in the plane perpendicular to the AB (x) axis.

c. Mirror plane including A and B . In this situation, the reflection does not swap sites and, choosing the mirror plane to be perpendicular to the axis z (and parallel to the axis x), one gets:

$$\begin{aligned} S_{A,x}S_{B,y} &\mapsto +S_{A,x}S_{B,y}, \\ S_{A,x}S_{B,z} &\mapsto -S_{A,x}S_{B,z}, \\ S_{A,y}S_{B,z} &\mapsto -S_{A,y}S_{B,z}. \end{aligned}$$

It follows that $\mathcal{J}_{xz}^{AB} = -\mathcal{J}_{xz}^{AB} \equiv 0$ and $\mathcal{J}_{yz}^{AB} = -\mathcal{J}_{yz}^{AB} \equiv 0$, while no symmetry constraints act on the component \mathcal{J}_{xy}^{AB} . The latter condition is compatible with the third Moriya's rule, stating that \mathbf{D} is perpendicular to the mirror plane xy , but a symmetric anisotropic part is also allowed for spin components lying within the same reflection plane.

d. Two-fold rotation axis perpendicular to AB and passing through C . Transformation rules imply that, for the two-fold rotation axis parallel to the axis z ($\perp x$):

$$\begin{aligned} S_{A,x}S_{B,y} &\mapsto +S_{B,x}S_{A,y}, \\ S_{A,x}S_{B,z} &\mapsto -S_{B,x}S_{A,z}, \\ S_{A,y}S_{B,z} &\mapsto -S_{B,y}S_{A,z}. \end{aligned}$$

It follows that the anisotropic exchange tensor can be decomposed in a purely antisymmetric part with \mathbf{D} perpendicular to the two-fold axis, as $\mathcal{J}_{xz}^{AB} = -\mathcal{J}_{zx}^{AB}$ and $\mathcal{J}_{yz}^{AB} = -\mathcal{J}_{zy}^{AB}$ (consistently with Moriya's fourth rule), as well as a purely symmetric part for spin components lying in a plane perpendicular to the rotation axis.

	inversion	m_{\perp}	m_{\parallel}	$C_{2\perp}$	$C_{n\parallel}$
D	= 0	\parallel mirror plane or $\perp AB$	\perp mirror plane	\perp two-fold axis	$\parallel AB$
K	$\neq 0$	$\parallel AB$	\perp mirror plane	\parallel two-fold axis	$\parallel AB$

TABLE S3: Generalized Moriya's rules for the anisotropic part of the exchange tensor, including both symmetric and antisymmetric components, described by the **K** and **D** vectors, respectively. All symmetry elements leave the C point bisecting the AB invariant, and their subscripts \perp and \parallel denote their corresponding orientation with respect to the AB direction.

e. Two-fold rotation axis parallel to AB. As for the case *c*, any rotation around an axis parallel to the bond AB does not swap sites, and for a two-fold rotation one gets:

$$\begin{aligned} S_{A,x}S_{B,y} &\mapsto -S_{A,x}S_{B,y}, \\ S_{A,x}S_{B,z} &\mapsto -S_{A,x}S_{B,z}, \\ S_{A,y}S_{B,z} &\mapsto +S_{A,y}S_{B,z}. \end{aligned}$$

It follows that $\mathcal{J}_{xy}^{AB} = -\mathcal{J}_{xy}^{AB} \equiv 0$ and $\mathcal{J}_{xz}^{AB} = -\mathcal{J}_{xz}^{AB} \equiv 0$, and no symmetry constraint exists on the \mathcal{J}_{yz}^{AB} component. Its antisymmetric part will give rise to a Dzyaloshinskii vector parallel to the bond axis x (as stated by the fifth Moriya's rule), while the symmetric part will couple spin components lying in a plane perpendicular to it.

The Moriya's rules extended also to the symmetric part of the anisotropic exchange tensor are summarized in Table S3, in terms of the Dzyaloshinskii vector **D** and the **K** vector introduced in the main text.

III. \mathcal{J} -MATRICES OF REPORTED STRUCTURES

Here we present the \mathcal{J} -matrices of the structures depicted in Fig. 2 of the Main Text and of the A_1A_2 , A_1B_2 , B_1A_2 and B_1B_2 sublattices of HT bilayer CrI_3 . $S = 3/2$ is used the energy mapping analysis. All the values are given in μeV units.

$$\mathcal{J}_{\text{LT1}} = \begin{pmatrix} *** & 0 & 0 \\ 0 & *** & 0 \\ 0 & 0 & *** \end{pmatrix}, \quad \mathcal{J}_{\text{LT2}} = \begin{pmatrix} *** & -17 & 24 \\ -16 & *** & -14 \\ 24 & -14 & *** \end{pmatrix}, \quad (\text{S2})$$

$$\mathcal{J}_{\text{HT1}} = \begin{pmatrix} *** & -168 & -50 \\ 168 & *** & 0 \\ 50 & -1 & *** \end{pmatrix}, \quad \mathcal{J}_{\text{HT2}} = \begin{pmatrix} *** & -4 & 166 \\ 4 & *** & -25 \\ -166 & -25 & *** \end{pmatrix}, \quad (\text{S3})$$

For HT structure the \mathcal{J}^{\dagger} tensor and its decomposition onto A and B sublattices

$$\mathcal{J}^{\dagger} = \begin{pmatrix} *** & 0 & 0 \\ 0 & *** & -18 \\ 0 & -18 & *** \end{pmatrix}, \quad (\text{S4})$$

$$\mathcal{J}_{A_1A_2}^{\dagger} = \begin{pmatrix} *** & -139 & -190 \\ 139 & *** & -29 \\ 190 & -29 & *** \end{pmatrix}, \quad \mathcal{J}_{A_1B_2}^{\dagger} = \begin{pmatrix} *** & -50 & -34 \\ -50 & *** & 2 \\ -34 & 2 & *** \end{pmatrix}, \quad (\text{S5})$$

$$\mathcal{J}_{B_1A_2}^{\dagger} = \begin{pmatrix} *** & 50 & 34 \\ 50 & *** & 2 \\ 34 & 2 & *** \end{pmatrix}, \quad \mathcal{J}_{B_1B_2}^{\dagger} = \begin{pmatrix} *** & 139 & 191 \\ -139 & *** & -29 \\ -190 & -29 & *** \end{pmatrix}, \quad (\text{S6})$$

[1] T. Moriya, Phys. Rev. **120**, 91 (1960), ISSN 1536-6065.